

Electronic Supplementary Information

Efficient Photoelectrochemical C-C coupling at BiVO₄ Electrodes under Visible Light Irradiation

William A. Swansborough-Aston,^a Ayman Soltan,^a Ben Coulson,^b Andrew Pratt,^b Victor Chechik,^a Richard E. Douthwaite^a

^aDepartment of Chemistry, University of York, York, YO10 5DD, UK.

^bDepartment of Physics, University of York, Heslington, York, YO10 5DD, UK

Contents

Materials and methods	2
Powder x-ray diffraction	3
Energy dispersive spectroscopy	4
X-ray photoelectron spectroscopy.....	5
Diffuse reflectance spectroscopy	7
GC headspace analysis.....	8
(Photo)electrochemistry.....	9
Electrochemical Impedance Spectroscopy	12
Apparent quantum yield (AQY) calculation	15
LSV and CPE of phenylacetic acid derivatives.....	16
CPE using a supporting electrolyte.....	19
GC calibration curves	20
References	22

Materials and methods

General: Bismuth (III) 2-ethylhexanoate and vanadyl (IV) acetylacetonate were purchased from Alfa Aesar. Ferrocene (98%) was purchased from Aldrich and purified by sublimation. FTO glass, triethylamine ($\geq 99.5\%$), 2-methyl, 4-methyl, 4-methoxy and 3-methoxyphenylacetic acid, benzoic and hydrocinnamic acids were purchased from Sigma-Aldrich. Phenylacetic acid (98.5 %) was purchased from Acros Organics. 3-chloro, 4-chloro and 4-fluorophenylacetic acid, 2-phenylisobutyric and 2-phenylpropionic acids were all purchased from Fluorochem. Tetrabutylammonium hexafluorophosphate was purchased from Fluka and was recrystallised in ethanol prior to use.

Powder x-ray diffraction

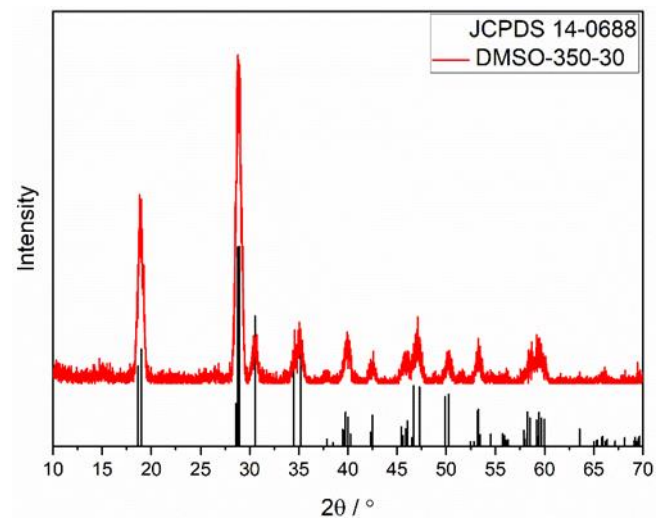


Figure S1. Grazing incidence X-ray diffractogram of a BiVO₄ photoelectrode.

Energy dispersive spectroscopy

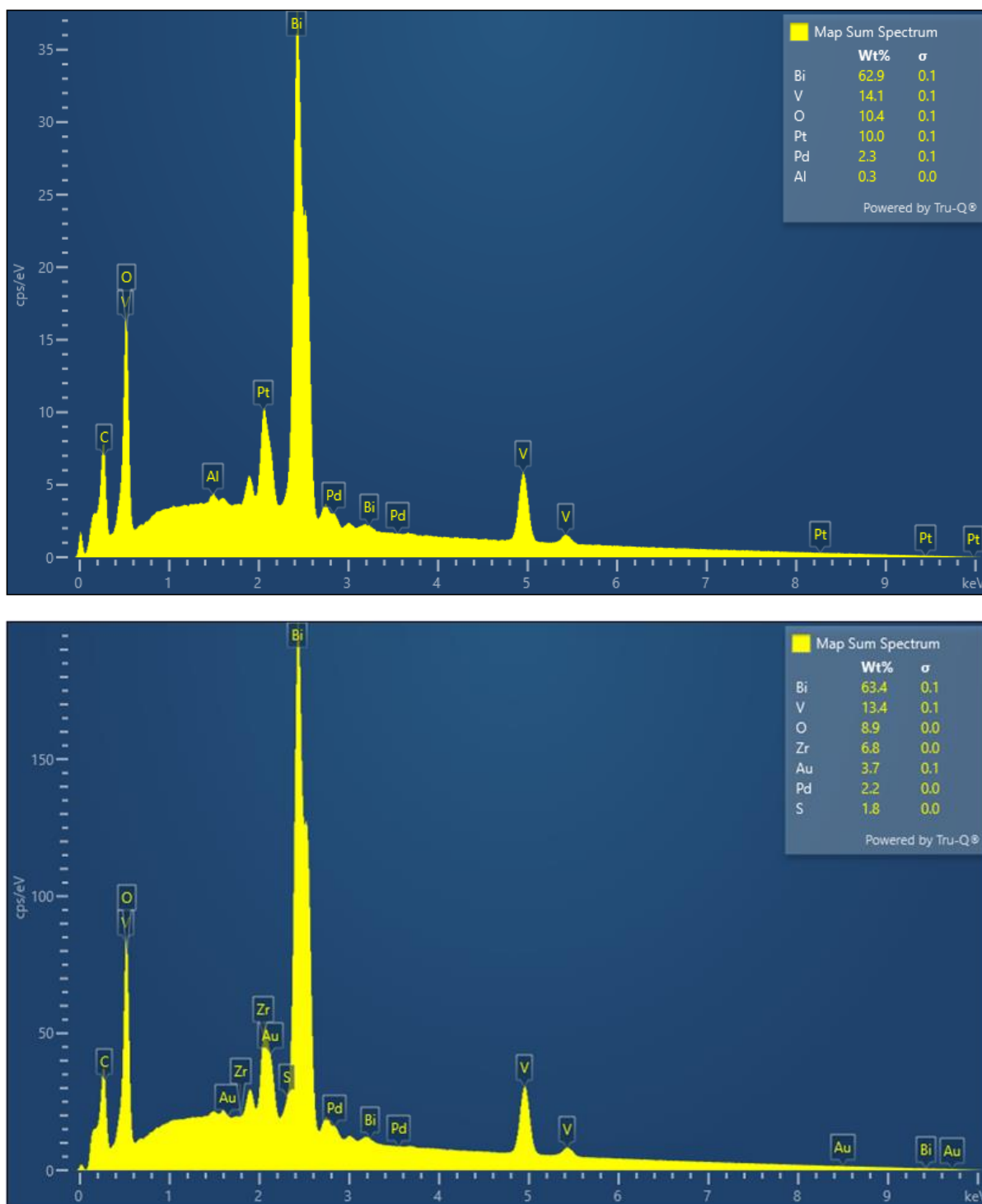


Figure S2. Energy dispersive X-ray spectrum of a BiVO₄ photoelectrode a) before use; b) after controlled potential electrolysis of 1 M PAA with 0.05 equiv Et₃N for 3 h at +0.09 V vs Fc/Fc⁺.

X-ray photoelectron spectroscopy

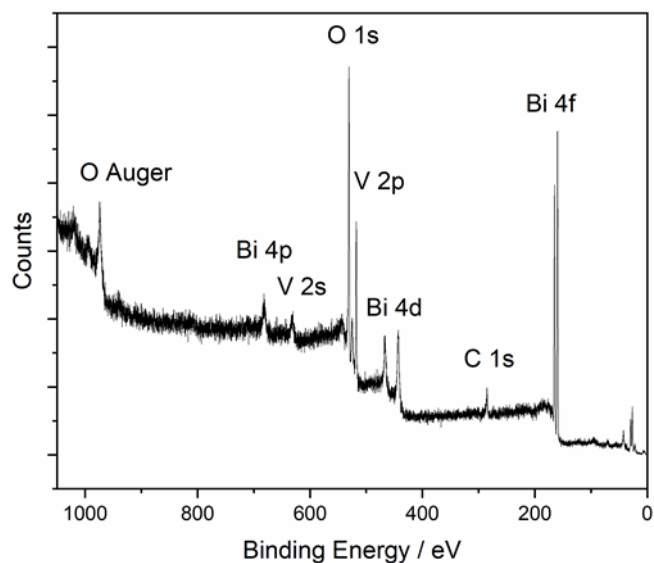


Figure S3. XPS survey spectrum of a BiVO_4 photoelectrode prepared by electrostatic spray pyrolysis.

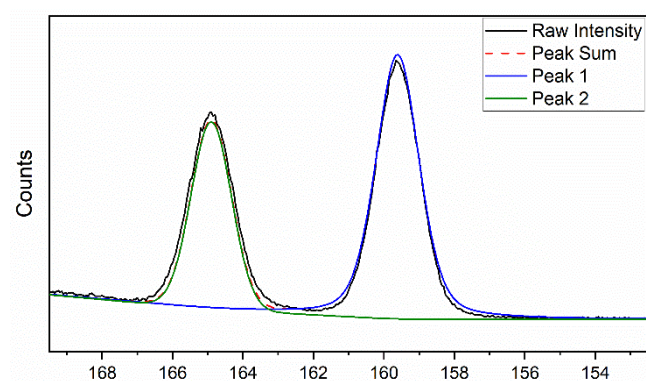


Figure S4. Bi 4f region and peak fitting of an XPS spectrum of a BiVO_4 photoelectrode.

Table S1. Summary of deconvoluted XPS signals in the Bi 4f region of the XPS spectrum.

Region	Peak	Species	Peak Position / eV	Peak FWHM / eV	Percentage Integration
Bi 4f	1	$\text{Bi}^{3+} 4f_{7/2}$	159.6	1.45	63.7
	2	$\text{Bi}^{3+} 4f_{5/2}$	164.9	1.35	36.3

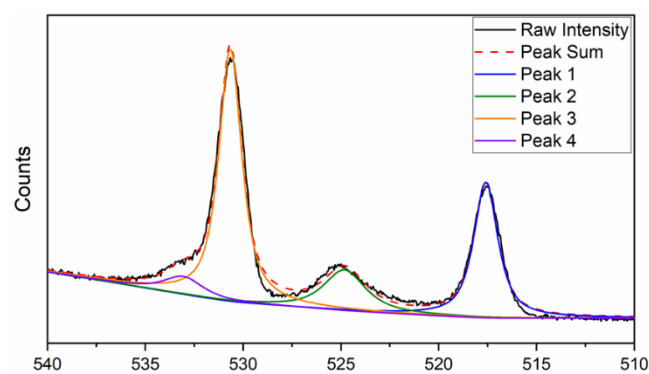


Figure S5. V 2p and O 1s regions and peak fitting of the XPS spectrum of a BiVO₄ photoelectrode.

Table S2. Summary of deconvoluted XPS signals in the V 2p and O 1s regions of the XPS spectrum.

Region	Peak	Species	Peak Position / eV	Peak FWHM / eV	Percentage Integration
V 2p	1	V ⁵⁺ 2p _{3/2}	517.6	1.47	28.6
	2	V ⁵⁺ 2p _{1/2}	524.8	2.54	14.8
O 1s	3	Metal Oxide	530.7	1.4	50.6
	4	Hydroxide/Water	533.1	2.35	6.1

Table S3. XPS quantification data of a BiVO₄ photoelectrode surface before controlled potential electrolysis of 1 M PAA with 0.05 equiv Et₃N for 3h at +0.09 V vs Fc/Fc⁺.

Peak	Centre	Integration	Factor	Int./Factor	Relative Quantity
Bi 4f	159.65	930	4.25	218	1
V 2p	517.6	551	1.3	424	1.93
O 1s	530.6	1138	0.66	1725	7.88

Table S4. XPS quantification data of a BiVO₄ photoelectrode surface after controlled potential electrolysis of 1 M PAA with 0.05 equiv Et₃N for 3h at +0.09 V vs Fc/Fc⁺.

Peak	Centre	Integration	Factor	Int./Factor	Relative Quantity
Bi 4f	159.85	952	4.25	224	1
V 2p	517.6	485	1.3	373	1.66
O 1s	530.6	1008	0.66	1528	6.82

Diffuse reflectance spectroscopy

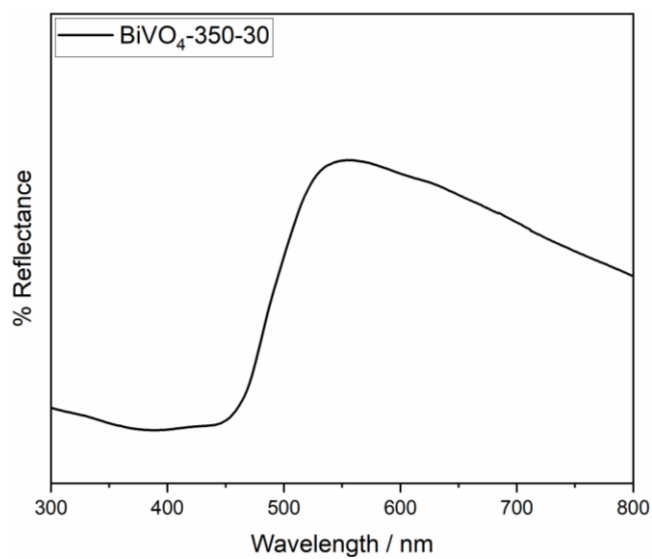


Figure S6. Diffuse reflectance spectrum of a BiVO₄ photoelectrode.

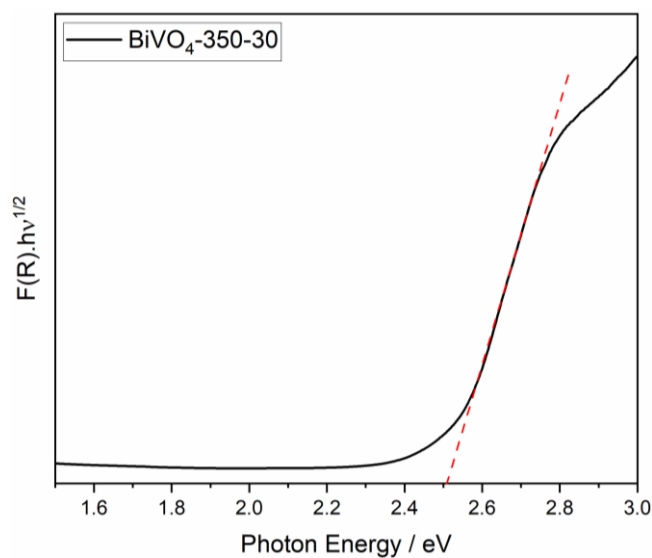


Figure S7. Tauc plot of a BiVO₄ photoelectrode showing a band gap of approximately 2.5 eV.

GC headspace analysis

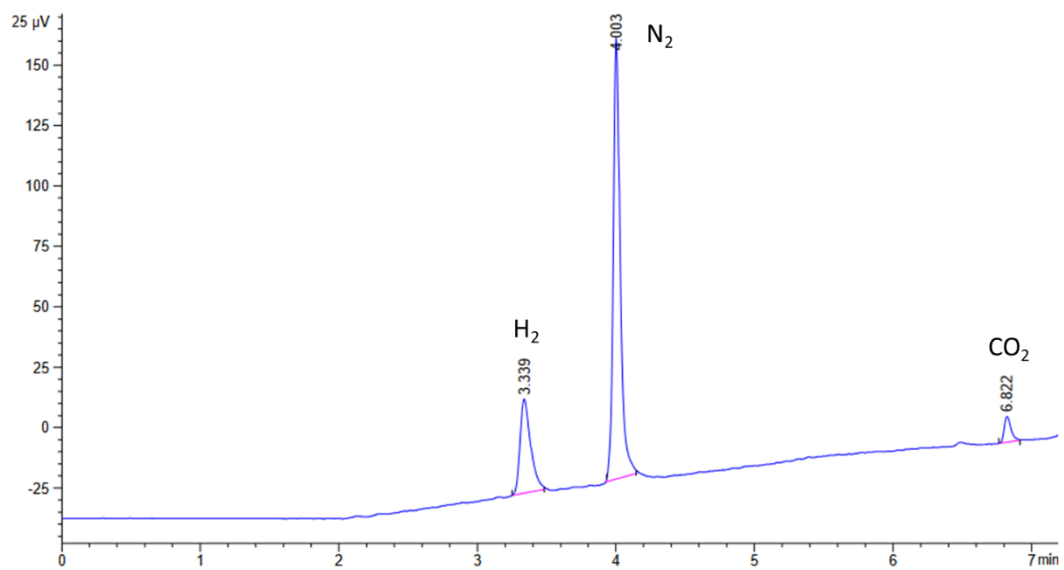


Figure S8. Gas chromatogram of the cell headspace after controlled potential electrolysis of 1 M PAA with 0.05 equiv Et₃N for 1h at +0.09 V vs Fc/Fc⁺.

(Photo)electrochemistry

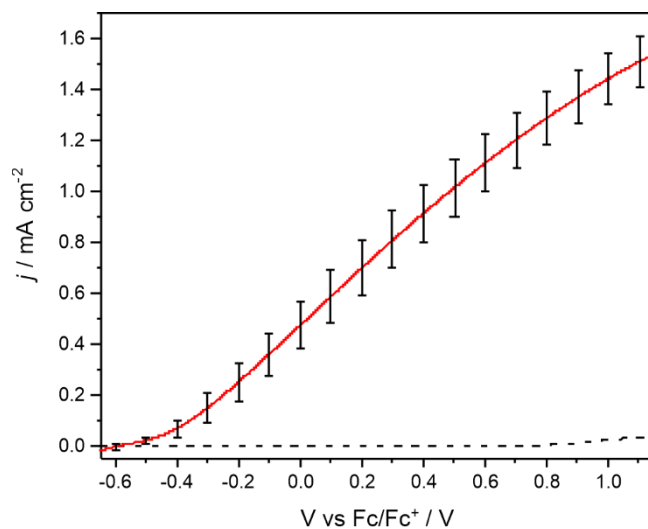


Figure S9. Average linear sweep voltammogram across 15 photoelectrodes in 1 M PAA and 0.05 equiv NEt_3 vs Fc/Fc^+ under illumination with AM 1.5G. Note all other experiments were performed using a blue LED array which gives larger photocurrents.

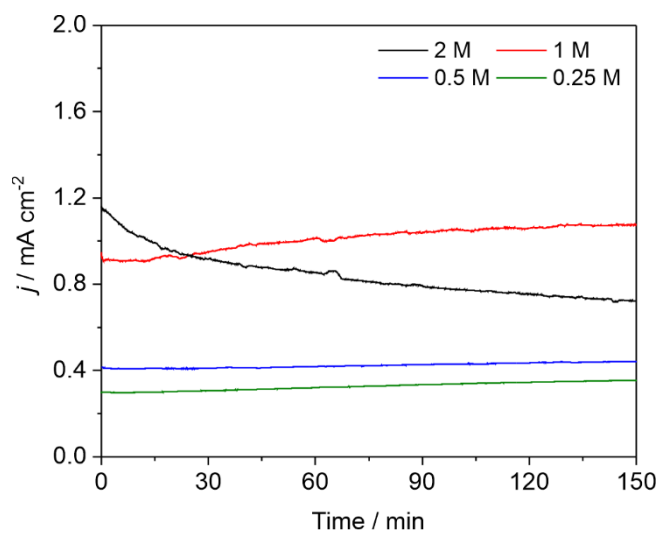


Figure S10. Controlled potential electrolyses of 2 M (black), 1 M (red), 0.5 M (blue) and 0.25 M (green) PAA electrolytes and 0.05 equiv Et_3N at +0.09 V vs Fc/Fc^+ .

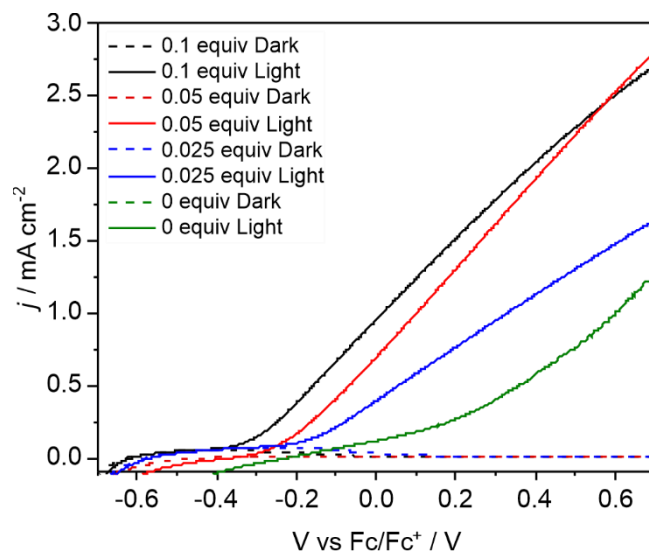


Figure S11. Linear sweep voltammograms of BiVO_4 photoelectrodes in electrolytes containing 1 M PAA with 0.1 (black), 0.05 (red), 0.025 (blue) and 0 equiv Et_3N (green). Voltammograms were recorded in the dark (dashed) and under blue LED illumination (solid). Scan rate 10 mV s^{-1} .

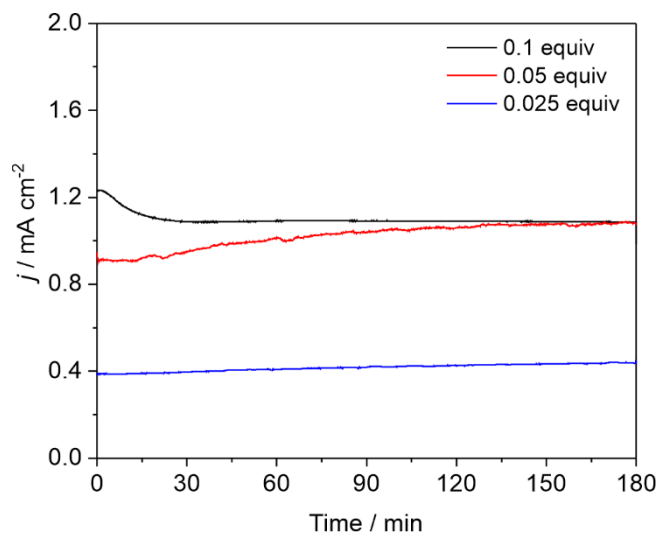


Figure S12. Controlled potential electrolyses of 1 M PAA solutions partially neutralised by addition of 0.1 (black), 0.05 (red) and 0.025 (blue) equiv Et_3N at $+0.09 \text{ V vs Fc/Fc}^+$.

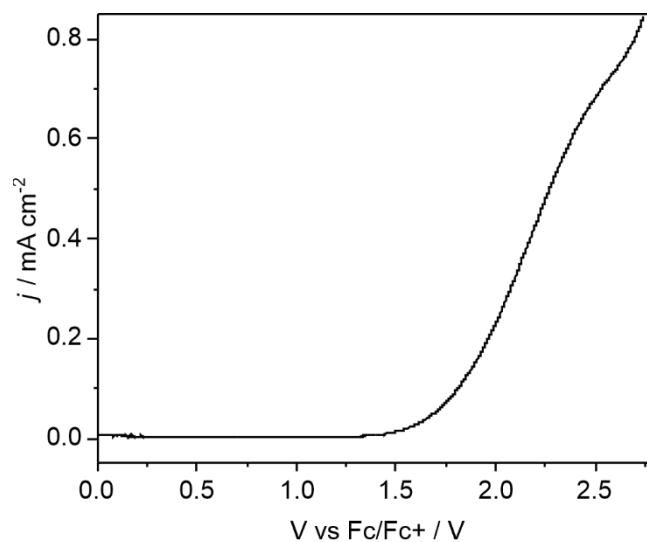


Figure S13. Linear sweep voltammogram in the absence of illumination of a BiVO_4 photoelectrode in 1 M PAA with 0.05 equiv Et_3N .

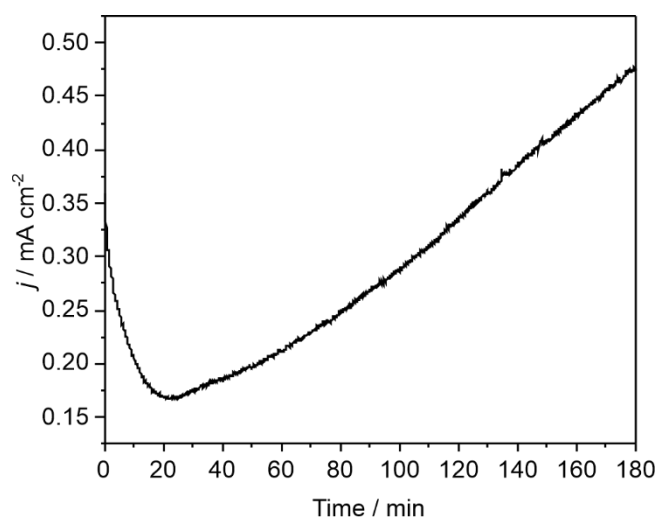


Figure S14. Controlled potential electrolysis in the absence of illumination of a BiVO_4 photoelectrode in 1 M PAA with 0.05 equiv Et_3N at 2.5 V vs Fc/Fc^+ .

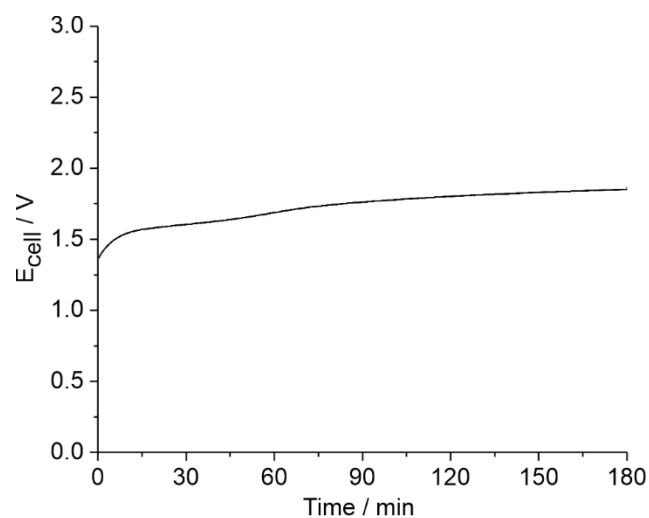
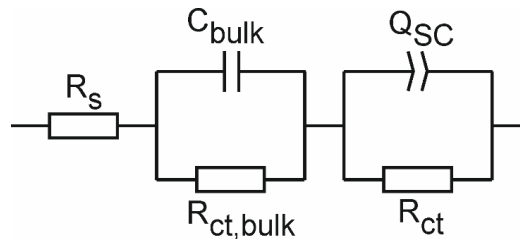


Figure S15. Cell voltage measured during controlled potential electrolyses of 1 M PAA solution partially neutralised by addition of 0.05 equiv Et_3N at +0.09 V vs Fc/Fc^+ .

Electrochemical Impedance Spectroscopy

Impedance spectra were initially fitted using a modified Randles cell, with cell series resistance, R_s , bulk capacitance, C_{bulk} , and bulk charge transfer resistance, $R_{\text{ct,bulk}}$, elements to model charge transfer within the semiconductor. A second constant phase element and resistor in parallel were added to model charge transfer resistance, R_{ct} , and space-charge capacitance, Q_{SC} , at the electrode surface.

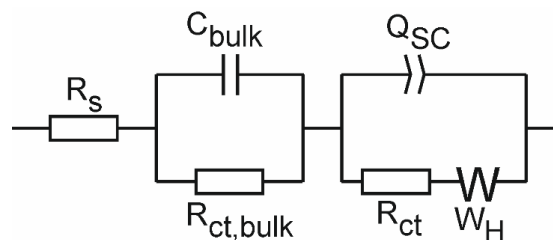


Capacitance values can be calculated from constant-phase elements using:

$$C_{\text{SC}} = \frac{(Q_{\text{SC}}R_{\text{ct}})^{1/n}}{R_{\text{ct}}}$$

Where C_{SC} is the space-charge capacitance and n is the constant phase element exponent, extracted from fitting of impedance data.¹The impedance response of porous films can be understood through the use of transmission line models, however correlating a large number of model parameters to real chemical processes is often difficult.^{2, 3} Similar equivalence cells have been used to model Fe_2O_3 photoelectrodes in photoelectrochemical C-H amination reactions in non-aqueous media.⁴

For the fitting of impedance spectra in 50 mM 4-Cl-PAA solutions, a similar equivalence cell as before was used, though a Warburg diffusion element, W_H , was included to account for the linear behaviour observed at low frequency caused by diffusion within the Helmholtz layer.



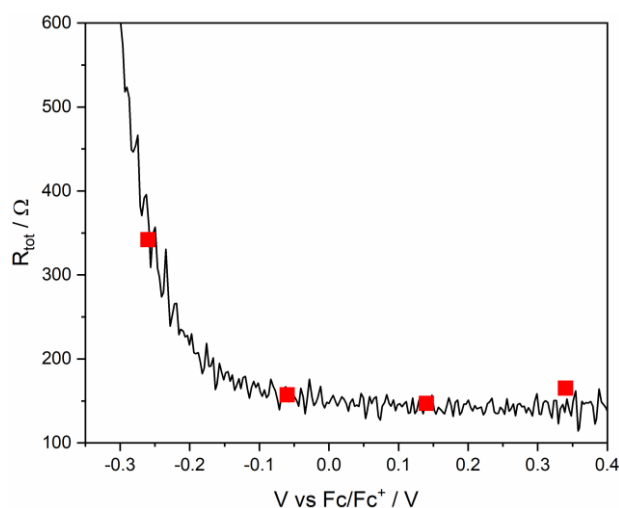


Figure S16. Total cell resistance (R_{tot}) calculated from linear sweep voltammograms of a BiVO_4 photoelectrode in 1 M 4-Cl-PAA electrolyte (black line). R_{tot} estimated from fitting of impedance spectra (red squares). The validity of impedance fitting using the equivalence cell shown in Fig. 5a was tested by comparison of total resistance, R_{tot} , measured by LSV and calculated from Table S6.⁵ For impedance measurements, R_{tot} was taken as the summation of all resistances ($R_s + R_{ct,bulk} + R_{ct}$). R_{tot} for LSV measurements was calculated using:

$$R_{tot} = \left(A_s \frac{dJ}{dV} \right)^{-1}$$

Where A_s is the electrode area, and dJ/dV is the differentiated voltammogram.

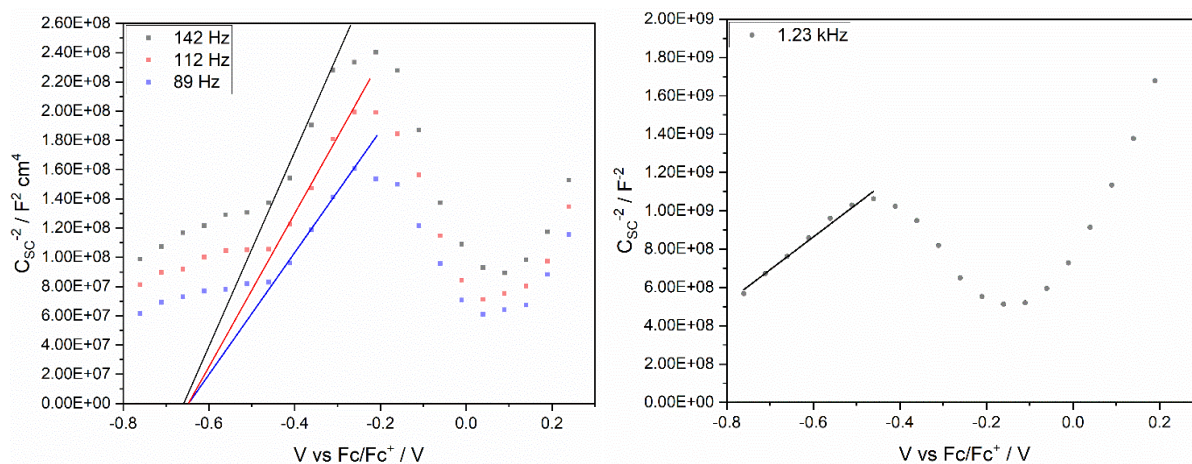


Figure S17. Mott-Schottky plots of a BiVO_4 photoelectrode in a) 1 M 4-Cl-PAA with 0.05 equiv Et_3N at 142 (black), 112 (red) and 89 Hz (blue); b) Mott-Schottky plot of a BiVO_4 photoelectrode in 0.05 M 4-Cl-PAA solutions containing 0.1 M TBAPF_6 . Due to the prevalence of the Warburg diffusion element at low frequency, Mott-Schottky plot was acquired at 1.23 kHz.

Table S5: Flat band potentials and donor densities of BiVO₄ photoelectrodes extracted from Mott-Schottky analysis. Donor density values were calculated using geometric area in absence of active surface area and a relative permittivity of $\epsilon = 86$.

[4-Cl PAA] ^a / M	Frequency / Hz	Flat Band Potential vs Fc/Fc ⁺ / V	N _D (x10 ¹⁹)/ cm ⁻³
1.0	142	-0.645	1.18
1.0	112	-0.644	1.48
1.0	89	-0.649	1.82
0.05 ^{a, b}	1230	-1.10	0.28

^a with added 0.05 equiv Et₃N, ^b with added 0.1 M TBAPF₆

Table S6. Comparison of parameters extracted from the fitting of impedance spectra for an illuminated BiVO₄ photoelectrode in 1 M and 0.05 M 4-Cl-PAA electrolyte.

[4-Cl PAA] ^a / M	V / V	R _s / Ω	C _{bulk} / μF	R _{ct,bulk} / Ω	C _{SC} / μF	R _{ct} / Ω
1.0	-0.26	53.12	0.972	8.226	380.8	280.8
1.0	-0.06	52.84	0.912	9.971	150.5	94.52
1.0	0.14	52.33	0.844	10.52	117.8	84.26
0.05 ^{a, b}	-0.06	19.64	39.5	6.37	422.4	430.9

^a with added 0.05 equiv Et₃N, ^b with added 0.1 M TBAPF₆

Apparent quantum yield (AQY) calculation

4-chlorophenylacetic acid (1.71 g, 10 mmol) was dissolved in dry, degassed MeCN (10 mL) and 0.05 equiv triethylamine (0.07 mL, 0.5 mmol) was added. 8 mL of this solution was added to a photoelectrochemical cell, with a 3-electrode configuration using a BiVO₄ working electrode, a Pt counter electrode, and an Ag wire reference electrode isolated in a Luggin capillary. Controlled potential electrolyses were undertaken at +0.09 V vs Fc/Fc⁺ for 1 min under blue LED illumination ($\lambda = 450$ nm, 32 mW cm⁻²). Incident photon to current efficiency (IPCE) was calculated as the ratio of photocurrent to the total number of photons irradiating the electrode.

$$\text{Number of Electrons} = \frac{ItN_A}{F}$$

Where i = photocurrent, t = time, N_A = Avogadro's number and F = Faraday constant

$$\text{Number of Incident Photons} = \frac{Y_e A \lambda}{hc}$$

Where Y_e = irradiance at the photoelectrode, A = geometric electrode area, λ = incident photon wavelength (450 nm), h = Planck's constant, and c = speed of light in a vacuum.

The apparent quantum yield (AQY) was calculated as the product of IPCE and Faradaic Efficiency for the Kolbe product.

For the electrolysis of 1 M 4-Cl-PAA under 32.2 mW cm⁻² irradiance:

$$\text{Number of Electrons} = \frac{2.1 \text{ mA} \times 1 \text{ s} \times 6.022 \times 10^{23}}{96485 \text{ s A mol}^{-1}} = 1.31 \times 10^{16}$$

$$\text{Number of Incident Photons} = \frac{32.2 \text{ mW cm}^{-2} \times 1.5 \text{ cm}^2 \times 450 \times 10^{-9} \text{ m}}{6.63 \times 10^{-34} \text{ m}^2 \text{ kg s}^{-1} \times 3 \times 10^8 \text{ m s}^{-1}} = 1.085 \times 10^{17}$$

$$\text{IPCE} = \frac{1.3 \times 10^{16}}{1.085 \times 10^{17}} \times 100\% = 12.1\%$$

$$\text{AQY} = 12.1\% \times 0.99 = 12.0\%$$

For context an IPCE = 100%, gives a theoretical $i = 17.4$ mA and $j = 11.6$ mA cm⁻².

Table S7. Light intensity dependence of 1 M PAA with 0.05 equiv. NEt₃ in acetonitrile.

Irradiance / mW cm ⁻²	Ave. Photocurrent @ +0.09 V vs Fc/Fc ⁺ / mA	Photon-to-Current Efficiency / %
32.2	2.10	12.1
16.5	1.81	20.2
9.70	1.28	24.2

LSV and CPE of phenylacetic acid derivatives

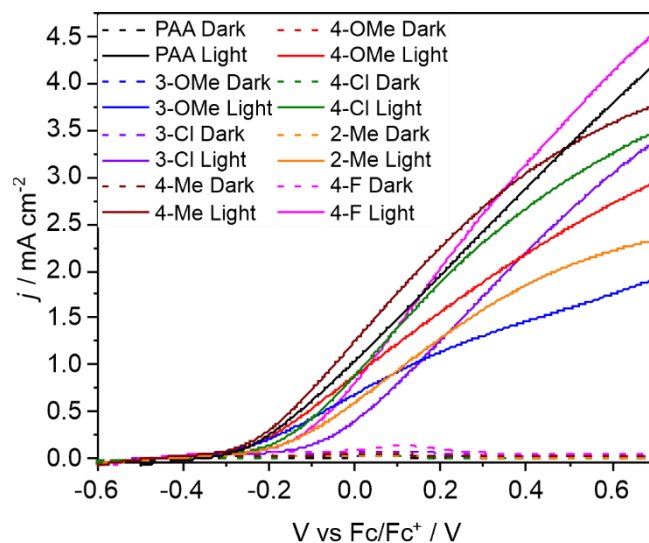


Figure S18. Linear sweep voltammograms of BiVO_4 photoelectrodes in 1 M of substituted phenylacetic acids with 0.05 equiv Et_3N compared to 1 M PAA (black). Voltammograms were recorded in the presence (solid) and absence (dashed) of blue LED illumination.

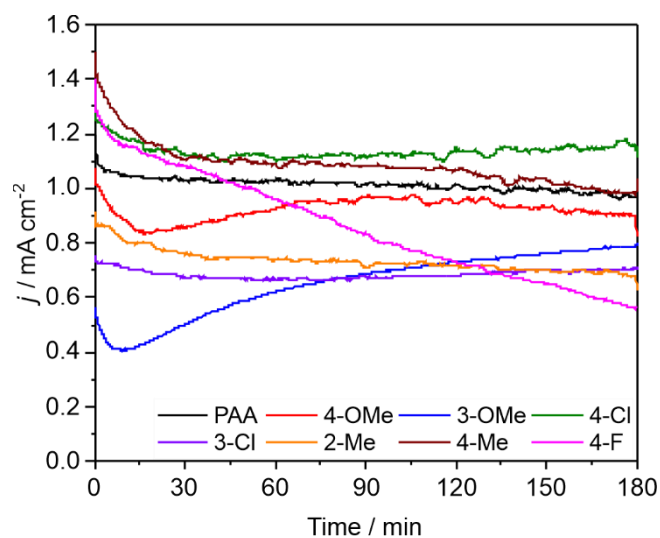


Figure S19. Controlled potential electrolyses of 1 M electrolytes of substituted phenylacetic acids with 0.05 equiv Et_3N at +0.09 V vs Fc/Fc^+ compared to 1 M PAA (black).

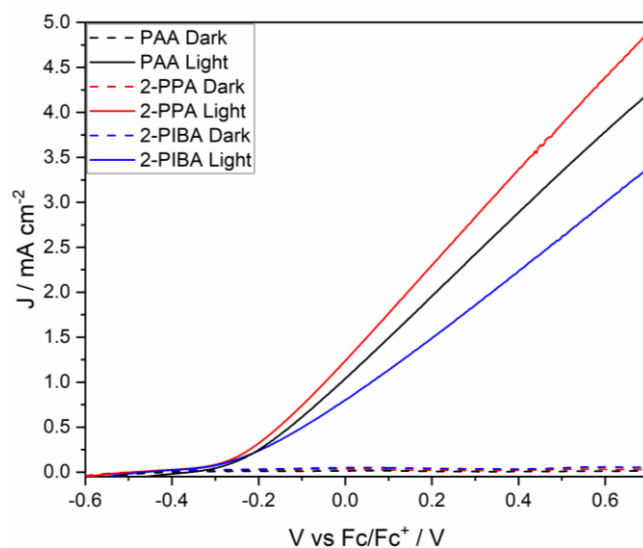


Figure S20. Linear sweep voltammograms of BiVO_4 photoelectrodes in 1 M 2-phenylpropionic (2-PPA, red) and 2-phenylisobutyric acids (2-PIBA, blue) with 0.05 equiv Et_3N compared with 1 M PAA (black). Voltammograms were recorded in the presence (solid lines) and absence (dashed lines) of blue LED illumination.

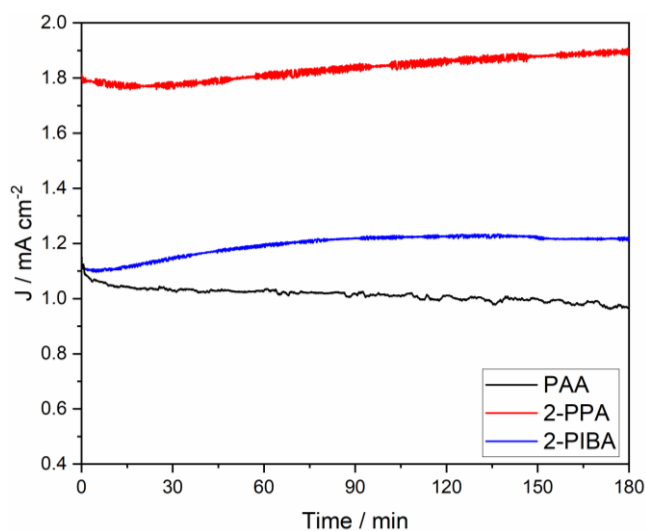


Figure S21. Controlled potential electrolyses of 1 M 2-phenylpropionic (red) and 2-phenylisobutyric acid (blue) with 0.05 equiv Et_3N at +0.09 V vs Fc/Fc^+ compared with 1 M PAA (black).

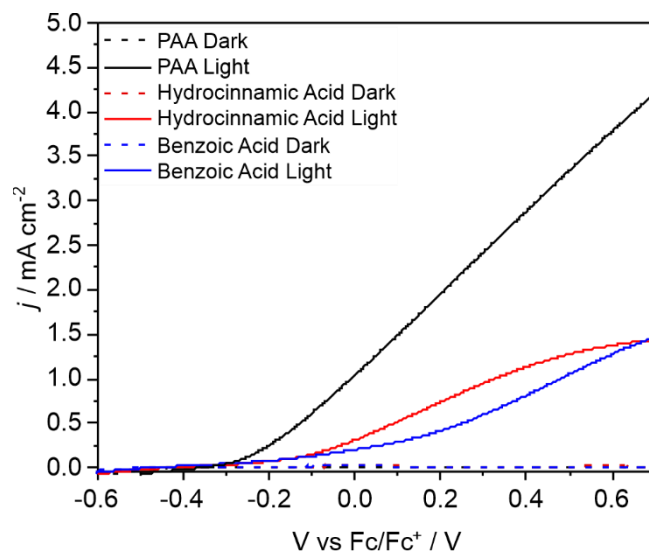


Figure S22. Linear sweep voltammograms of a BiVO_4 photoelectrode in 1 M 3-phenyl propanoic (red) and benzoic (blue) acids with 0.05 equiv Et_3N compared to 1 M PAA (black). Voltammograms were recorded in the presence (solid) and absence (dashed) of blue LED illumination.

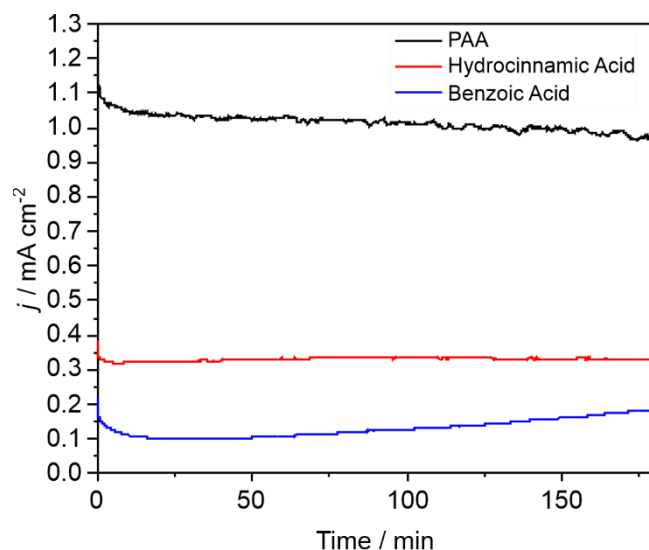


Figure S23. Controlled potential electrolyses of 1 M hydrocinnamic (red) and benzoic (blue) acids with 0.05 equiv Et_3N at +0.09 V vs Fc/Fc^+ compared to 1 M PAA (black).

CPE using a supporting electrolyte

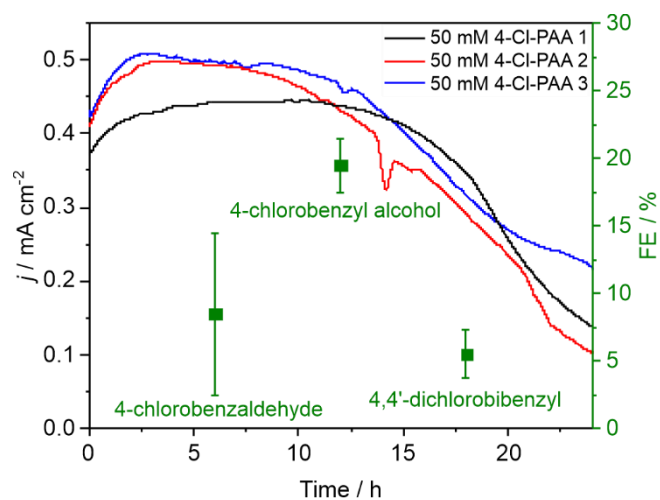


Figure S24. Controlled potential electrolyses using three electrodes of electrolytes containing 0.1 M TBAPF₆, 0.05 M 4-Cl-PAA and 0.05 equiv Et₃N at +0.25 V vs Fc/Fc⁺ under blue LED illumination.

GC calibration curves

Bibenzyl, benzyl alcohol and benzaldehyde were dissolved in 1:1 CH₂Cl₂:MeOH and chromatograms recorded in triplicate at each concentration.

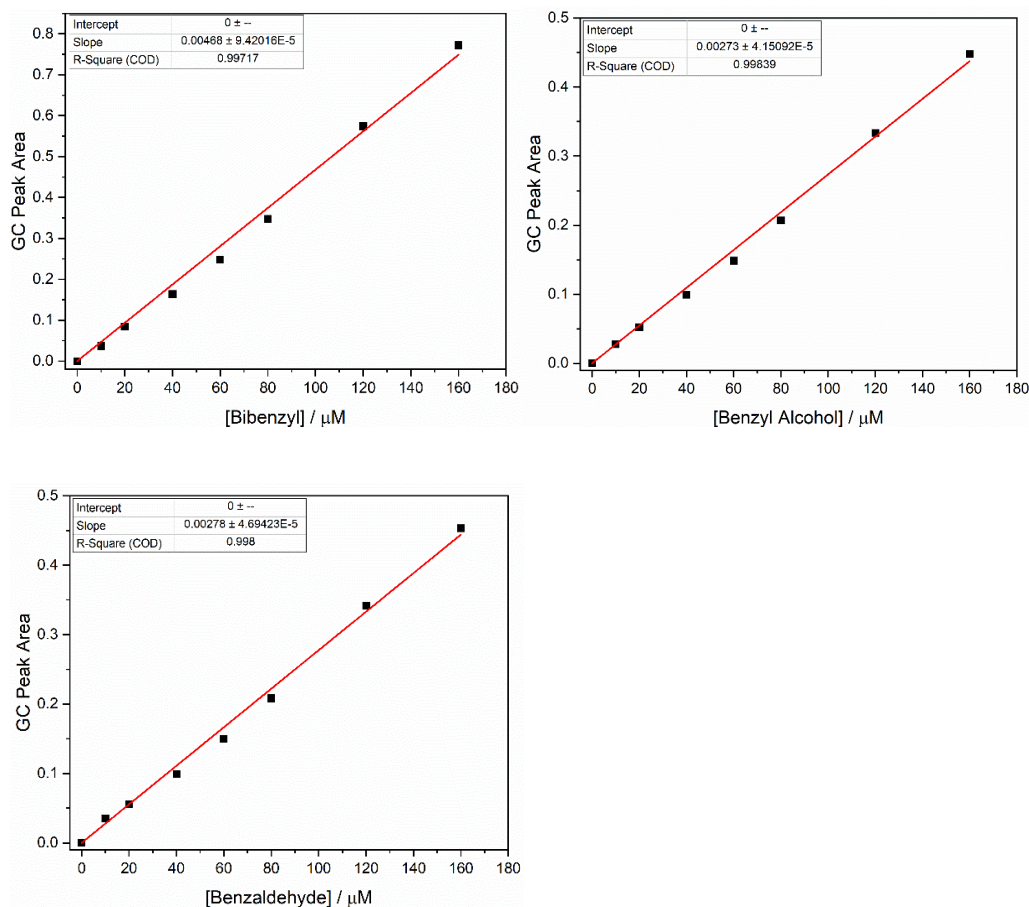


Figure S25. GC calibration curves for bibenzyl, benzyl alcohol, and benzaldehyde.

Table S8. GC retention times of acid starting materials, Kolbe and non-Kolbe products

Acid	Aldehyde r.t. / min	Alcohol r.t. / min	C-C Kolbe r.t. / min	Acid r.t. / min
PAA	4.57	5.08	8.84	6.24
4-OMe-PAA	7.12	7.32	nd	8.50
3-OMe-PAA	6.22	6.55	nd	8.35
4-Cl-PAA	nd ^a	nd	11.94	7.79
2-Me-PAA	5.71	5.96	10.34	7.05
4-Me-PAA	5.81	6.22	10.22	7.02
3-Cl-PAA	5.82	6.83	11.73	7.76
4-F-PAA	4.46	5.13	8.71	6.13
2-PPA	nd	nd	9.26, 9.36 ^b	6.45
2-PIBA	nd	nd	10.95	6.81
Benzoic	nd	nd	nd	5.47
Hydrocinnamic	nd	5.43	nd	6.88

^aNone detected. ^bretention times of diastereomers.

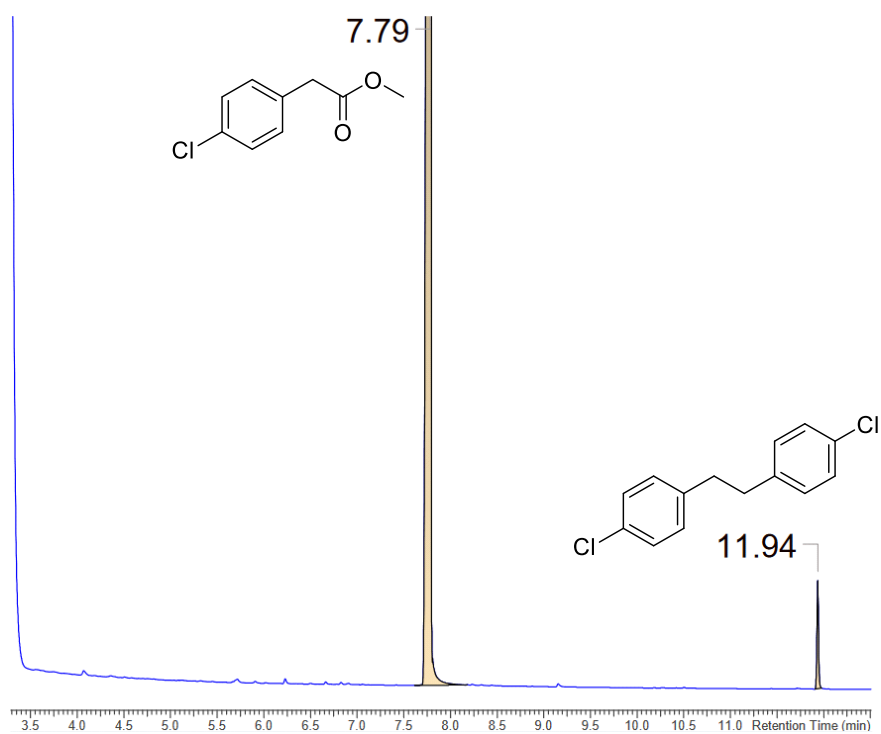


Figure S26. Example chromatogram of 4-Cl-PAA electrolysis products after 3 h at +0.09 V vs Fc/Fc⁺.

References

1. M. E. Orazem and B. Tribollet, *Electrochim. Acta*, 2008, **53**, 7360-7366.
2. J. Bisquert, G. Garcia-Belmonte, F. Fabregat-Santiago, N. S. Ferriols, P. Bogdanoff and E. C. Pereira, *J. Phys. Chem. B*, 2000, **104**, 2287-2298.
3. F. Fabregat-Santiago, G. Garcia-Belmonte, J. Bisquert, A. Zaban and P. Salvador, *J. Phys. Chem. B*, 2002, **106**, 334-339.
4. L. Zhang, L. Liardet, J. Luo, D. Ren, M. Grätzel and X. Hu, *Nat. Catal.*, 2019, **2**, 366-373.
5. B. Klahr, S. Gimenez, F. Fabregat-Santiago, T. Hamann and J. Bisquert, *J. Am. Chem. Soc.*, 2012, **134**, 4294-4302.